Stimulated Brillouin Scattering in Bulk crystalline resonator

Semester Thesis

Hugo Banderier

`hbanderier@student.ethz.ch`

March 13, 2021

Abstract

Information stored as phonons in bulk crystalline resonators offers the unique advantage to be accessed optically through Stimulated Brillouin Scattering (SBS) on top of the conventional piezoelectric interaction. This additional way to control these long-lived, high quality factor modes offers a new path towards deterministic qubit signal transduction in addition to applications in precision metrology. The central quantity that needs to be determined when working in this new scheme is the so-called Brillouin frequency of the crystal used. In this thesis, we explain the theory of stimulated Brillouin scattering and describe the apparatus needed to measure the Brillouin frequencies of crystals.

Contents

Introduction

1.1 Motivation

Phononic resonators in the quantum regime offer a path towards scalable quantum information processing thanks to their foreseen applications as interface between optical and microwave regimes [1] [2] [3][4] and long lived storage [5], and size advantage over their electromagnetic counterparts [6][7]. Fine control over long lived phonon modes has thus been the aim of the past 15 years of study in optomechanics, with great results such as ground state cooling, single phonon level control [8], mode splitting[9] and local entanglement [10] [11] coming from micro- and nanoscale resonators supporting surface accoustic waves during the last decade.

The two most explored ways to access a mechanical resonators electromagnetically are electromechanical interactions like piezoelectricity and optomechanical interactions like Brillouin scattering. In optomechanics, the light is virtually always supplied by a laser. One of the principal limitation of optomechanical devices is heating coming from the laser driving it, causing quick decoherence. The use of a macroscopic crystal supporting bulk accoustic waves allows greatly reduced surface interactions and mitigates laser heating, which may allow for more involved experiments. They also allow for a novel way of accessing phonon modes using stimulated Brillouin scattering, which make them most enviable for microwave-to-optical transduction schemes, central in the idea of distributed quantum computing and quantum internet.

With this new framework in mind, the production of specialized hybrid quantum devices centered around bulk crystalline optomechanics is under way in several groups. These devices use crystals whose central quantity of interest, in this framework, is the Brillouin frequency, the frequency of resonant three-wave mixing. This frequency needs to be known with the best possible certainty to make good use of these devices.

Here, we are interested in an experiment setup used to measure the highest fQ product in a coherent phonon accessed by a laser through SBS [12]. We will use this setup as a Brillouin spectrometer for this goal. We will first quickly go over the theory of stimulated Brillouin scattering, then explain in detail the experimental setup. We will cover mounting the crystal in the 4.2 K He cryostat and performing the cooldown, free-space alignment, fiber optics active and passive devices setup, and measurement scheme.

Theory

2.1 Stimulated Brillouin scattering

Stimulated Brillouin Scattering (SBS) is a three wave mixing process. In this report, we will only consider SBS involving a right moving Stokes phonon (Ω_s, $\vec{q}_s$) and two counter-propagating and detuned photons that we label pump (ω_p, $\vec{k}_p$, right-moving) and probe, red-detuned from pump ($\omega_s < \omega_p$, $-\vec{k}_s$, left-moving). Conservation of energy and momentum respectively imply $\Omega_s = \omega_p - \omega_s$ and $\vec{q}_s = \vec{q}(\Omega_s) = \vec{k}_p + \vec{k}_s$ where $q(\Omega) = \frac{\Omega}{v_a}$ is the dispersion relation for the acoustic mode, assumed to be linear as well as the optical one, with v_a and v_o the respective acoustic and optical phase velocities. Solving these equations together yield [13]

$$\Omega_B = \frac{2\omega_p v_a/v_o}{1 + v_a/v_o} \approx 2\omega_p v_a/v_o \tag{2.1}$$

This configuration of SBS is referred to as SBS amplifier. As such, the bandwidth Γ of
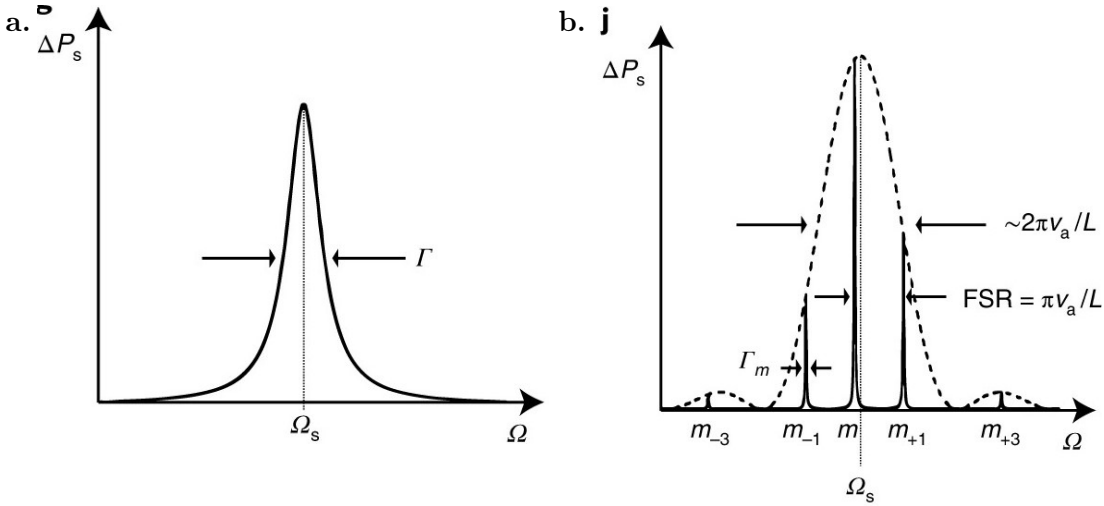

Figure 2.1: Gain spectra at (a) room temperature and (b) cryogenic temperature, from [12]

Lorentzian shown in the amplification spectrum of figure 2.1.a is called gain bandwidth. At room temperature, these created Stokes phonons have a typically short decay length

($\sim 100\mu m$), but can be created at any frequency and wavevector uniquely defined by the conservation equations. At cryogenic temperatures, the decay lengths of the created phonons are much longer than a round trip in the crystal. Since the faces of the crystal act like mirrors, the crystal becomes a phononic cavity of FSR given by its size and speed of sound supporting a discrete set of modes of frequencies, wavevectors and bandwidths $\{\Omega_m, \vec{q}_m, \Gamma_m\}$.

2.2 Sidebands signature

In order to better our measurement scheme, as done in [12], we use lock-in detection which, as described in section 3.4.2, requires the output signal to be modulated at known detuning Δ. To do this, we modulate the pump light before it enters free space to create sidebands in its spectrum, which are then imprinted on the output light during SBS in the crystal. The way this imprinting works at either cryogenic or room temperature is not exactly trivial and worth being explained.

Room temperature imprinting The incident modulated pump, scattered Stokes and acoustic fields have the following respective general expression in the medium if we assume only first order sidebands for each field :

$$\mathbf{E}_p(z,t) = [E_{p-1}(z)e^{i\Delta(t-z/v_o)} + E_{p0}(z) + E_{p+1}(z)e^{-i\Delta(t-z/v_o)}]e^{i(k_p z - \omega_p t)}\hat{x} + \text{c.c.}, \quad (2.2)$$

$$\mathbf{E}_s(z,t) = [E_{s-1}(z)e^{i\Delta'(t+z/v_o)} + E_{s0}(z) + E_{s+1}(z)e^{-i\Delta'(t+z/v_o)}]e^{i(-k_s z - \omega_s t)}\hat{x} + \text{c.c.} \quad (2.3)$$

$$\mathbf{u}(z,t) = [b_{-1}(z)\mathrm{e}^{i\Delta''(t-z/v_a)} + b_0(z) + b_{+1}(z)\mathrm{e}^{-i\Delta''(t-z/v_a)}]\mathrm{e}^{i(q_0 z - \Omega_B t)}\hat{z} + \text{c.c.} \quad (2.4)$$

with light band amplitudes $E_\gamma, \gamma = p-1,\ p,\ p+1,\ s-1,\ s,\ s+1$, accoustic band amplitudes $b_{0,\pm 1}$ and detunings $\Delta, \Delta', \Delta''$ which are not necessarily equal.

Even though SBS is a continuous process, for this part it is easier to see as a 2-step process that repeats. The incident Stokes light does not yet have any sideband when it first reaches the crystal : $E_{s-1}(z=L) = E_{s+1}(z=L) = 0$. In step one, phonons of bands (0, $\pm$1) are respectively created by interactions between $E_{p(0,\pm 1)}$ and E_{s0}. From conservation of energy we directly get that the side phonon modes are created with the same modulation as the pump : $\Omega_B \pm \Delta'' = \omega_p \pm \Delta - \omega_s \implies \Delta'' = \Delta$, where Δ'' is the modulation of the phonon sidebands. Note that we are usually not in a resolved sideband regime since $\Gamma_{\text{phonons}} \sim 10$ MHz, bigger than typical values of $\Delta \sim 100$ kHz.

In step 2, the pump modes and the freshly created phonons conspire to create new Stokes light. A pump mode and a phonon with the same detuning (from ω_p and Ω respectively) will create Stokes light in the main band (ω_s). A pump mode scattering on a blue-detuned phonon will create a red-detuned Stokes photon at frequency $\omega_s - \Delta'$. In the picture of figure 2.2 step 2, this corresponds to the interaction between p_0 and b_{+1} and the interaction between p_{-1} and b_0 that both create light on the s_{-1} mode. It can be shown that $\Delta' = \Delta\left(\frac{1+\frac{v_a}{v_o}}{1-\frac{v_a}{v_o}}\right) \approx \Delta$ since $\frac{v_a}{v_o} \sim 10^{-5}$. In the real picture, these two steps
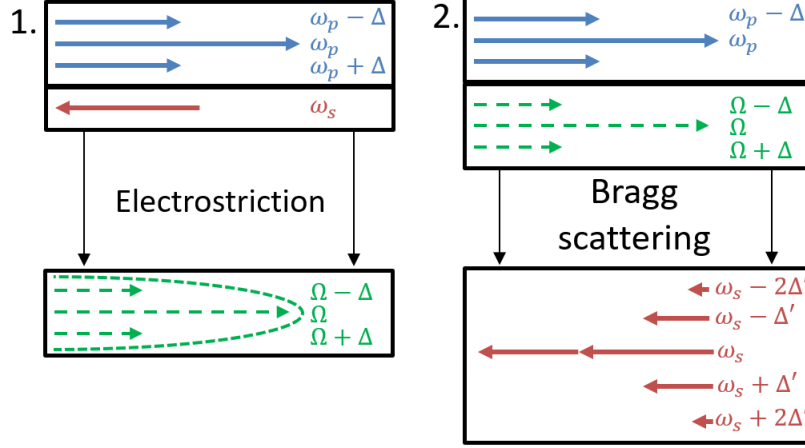
Figure 2.2: Illustration of the two first "steps" of signature imprinting at room temperature.

are of course simultaneous continuous processes that feed each other to amplify Stokes light more and more in further and further sidebands.

Cryogenic temperature imprinting   In this situation, we consider a single resonant phonon mode Ω_m within the gain bandwidth. The interaction Hamiltonian is

$$
H^{\text{int}} = \int_0^L \, \mathrm{d}z g_0 e^{i(q_0 - \Delta k)z} A_{p0}^\dagger A_{s0} b_0 + \int_0^L \, \mathrm{d}z g_0 e^{i(q_0 - \Delta k_{-1})z} A_{p-1}^\dagger A_{s-1} b_0
$$
$$
+ \int_0^L \, \mathrm{d}z g_0 e^{i(q_0 - \Delta k_{+1})z} A_{p+1}^\dagger A_{s+1} b_0 + \text{c.c.} \quad (2.5)
$$

where $\gamma = p - 1,\ p,\ p + 1,\ s - 1,\ s,\ s + 1$, $b_0(t)$ is the amplitude operator for the standing phonon mode, $A_\gamma(z,t)$ is the mode envelope operator for the optical field and $\Delta_{k\pm 1} = k_{p\pm 1} + k_{s\pm 1}$. To solve this Hamiltonian, it makes things easier to assume that the intensity beat length is much longer than the crystal length (verified in our setup, see 3.3.2) $|q_0 - \Delta k_{\pm 1}| = \frac{2\Delta}{v_0} \ll \frac{1}{L}$. This results in the following steady-state solutions for the modes :

$$
\bar{b}_0 \simeq -\frac{2i}{\Gamma_0} \int_0^L \, \mathrm{d}z g_0^* \bar{A}_{s0}^\dagger \bar{A}_{p0} \tag{2.6}
$$

$$
\frac{\partial \bar{A}_{s0}}{\partial z} \simeq g_0^* \bar{b}_o^\dagger \bar{A}_{p0} \tag{2.7}
$$

$$
\frac{\partial \bar{A}_{s\pm 1}}{\partial z} \simeq g_0^* \bar{b}_o^\dagger \bar{A}_{p\pm 1} \tag{2.8}
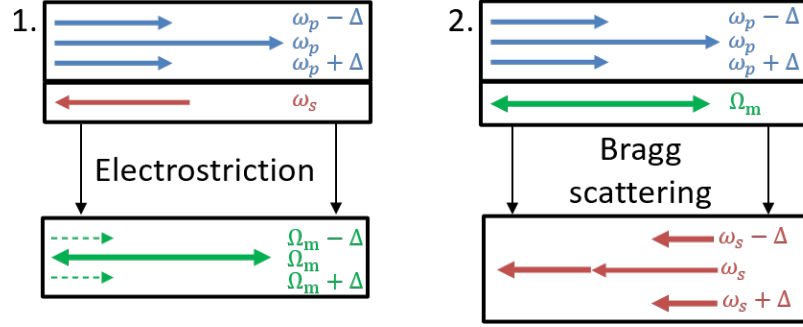$$

Figure 2.3: Illustration of signature imprinting through a single resonant long-lived phonon mode at cryogenic temperatures. The other excited phonons die much faster than the resonant one, having a negligible contribution to the amplification process.

with $\bar{A}_\gamma = A_\gamma e^{i\omega_\gamma t}$, $\bar{b}_0 = b_0 e^{i\Omega_m t}$. Put into words, it describes a similar but simpler situation than at room temperature. Phonons on the mode ($\bar{b}_0$ at Ω_m) far outlive the ones created at non resonant frequencies, so the analysis only has to focus on it. Then the Bragg scattering happens between the ($p0$, $p-1$, $p+1$) pump mode and the resonant phonons to create the ($s0$, $s-1$, $s+1$) Stokes mode respectively. At $z = 0$, the end of the Stokes photon's travel inside of the crystal, we can derive

$$A_{s\pm1}(0) = -\frac{2i\,|g_0|^2\,L^2}{\Gamma_0 v_o} A_{p0}(0)^* A_{p\pm1}(0) A_s(L). \qquad (2.9)$$
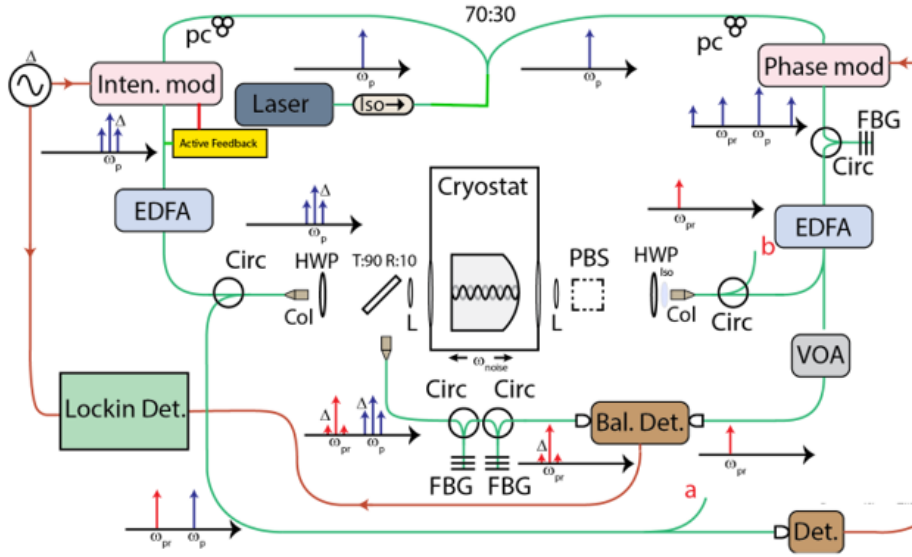
Experimental setup

Figure 3.1: Full experimental setup for Brillouin spectroscopy, modified from [12]

The full experimental setup, modified from, can be seen on figure 3.1. It features the free space setup with the cryostat in the middle, the pump arm with the intensity modulator on the left, the probe arm with the phase modulator and FBG bandpass filter on the right and the output arm with the π-phased FBGs, the balanced detector and the lock-in detection at the bottom.

3.1 Cryogenics and crystal mounting

As one can see on fig 3.1, the crystal is mounted inside a cryostat in the middle of the free space part of the setup. The cryostat we use uses a continuous liquid Helium flow to cool down the sample to 4.2 K and has sufficient cooling power (~ 1 W) to negate the heating from the lasers at typical operation powers of up to 200 mW, out of which no more than 10% has been observed to scatter in the cryostat. The device is simply a vacuum chamber with an inside chamber in which the sample is attached to a cold finger

and the Helium flows. It features small windows at the same height as the sample so the laser can reach the sample and the vacuum chamber has anti-reflection windows at the same level.

The crystal is mounted on the cold finger using a copper T-piece that came with the cryostat, and homemade copper holders. The temperature is recorded both at the cold finger and on the copper holder, using Cernox temperature sensors. The copper-beryllium holders are coated with vacuum grease and tightly screwed onto the crystal to maximize thermalization.
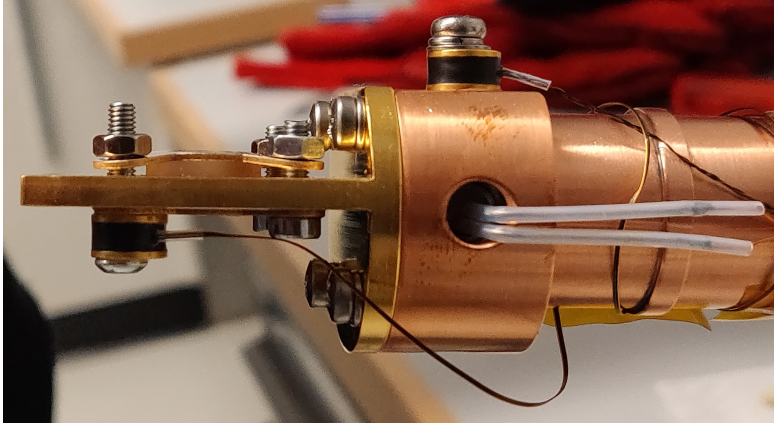

Figure 3.2: End of the cold finger, copper T-piece and crystal attached to it using home made copper holders.

The crystal's sides are also coated with vacuum grease since it touches the edges of the hole in the T-shaped piece in which it lies. Unfortunately we cannot get the exact temperature of the crystal itself, only that of the holders, so we cannot check that the crystal is indeed at the temperature we wish it to be. Nevertheless all the efforts that have been made to thermalize it make us confident its temperature does not go too far from the holder's. A heating wire is also present, which could potentially be used in the future to study the temperature dependency of the measured quantities. A flat-flat z-cut quartz held by this holder assembly can be seen on figure 3.2

3.2 Free space optics

3.2.1 Setup

On the optical table, the free-space part of fig 3.1 can be seen on figure 3.3. It features in- and out-couplers, mirrors, lenses and a beam splitter to form the three arms : Pump, probe and output. It also has polarization optics to match the polarization of both input lights, tested before the actual experiment using a polarizing beam splitter in the empty post at the end of the probe arm. An optical isolator can be placed in front of the probe in-coupler to avoid stimulated Brillouin scattering from happening in this fiber, which would add another Brillouin signal just like the one we are looking for (but much stronger, see 4.2), at a modulation Ω equal to the fiber's Brillouin frequency of ~ 10.8 GHz.
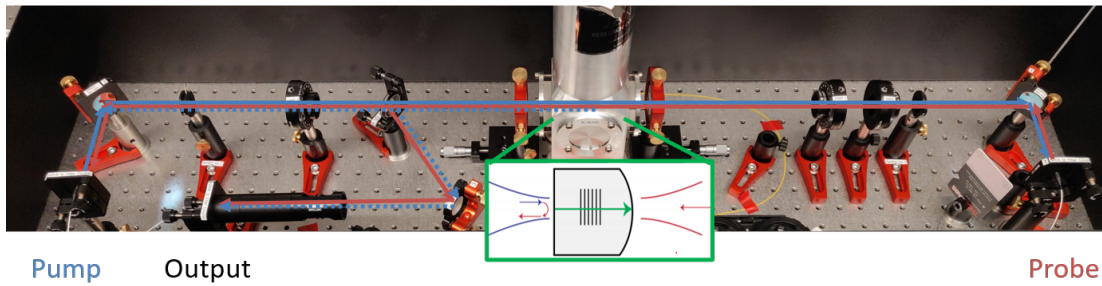
Figure 3.3: Free-space optics setup featuring all 3 (pump, probe and output) couplers, polarization optics and the cryostat.

3.2.2 Alignment

To align all of these components, we follow the following procedure :

1. Remove the middle lenses, connect both probe and pump in couplers to a laser. Visible light handheld laser can be very helpful for the next step, or high power IR using an EDFA.

2. Using photosensitive card and with all 8 degrees of freedom available (position and angle of both arms), make both lasers go through both pinholes and sit on top of each other. For fine-tuning the alignment, have one laser on one side and a handheld fiber power meter after the other side's coupler, and maximize the outcoupled power.

3. Add the probe arm lens and look for the crystal's back reflection near the probe-size pinhole or the wave-plates. Rotate the cryostat top part (connected to the cold finger) if there is no vacuum, otherwise rotate the whole cryostat until the back-reflected light sits on top of the incident one. Tightening the top part should make up for any vertical misalignment otherwise the mounting needs to be redone. This ensures the light is hitting the crystal perpendicularly.

4. To fine tune, use a circulator before the incoupler, with light coming in port 1, the incoupler on port 2 and a photodetector on port 3. Have the input laser sweep frequency over a few 100s of GHz range. The crystal forms a very lossy optical cavity with predictable FSR. One can maximize contrast between dips and peaks, i.e. quality factor of the cavity, on the quickly refreshing spectrum to ensure the alignment is as good as possible.

5. Add the second lenses and align them such that the optical path remains the same if possible. One can connect a laser on the pump arm and a power meter after the probe arm coupler and maximize the power by only moving the lenses' degrees of freedom.

6. Minimize probe light transmission of the film beam splitter by rotating the half- and quarter-wave plate.

7. Maximize both probe and pump arm reflection of the polarizing beam splitter. The previous step should make the probe arm's polarization already close to optimal. This ensures both lights have the same polarization.

8. Align the third arm by maximizing the power out coupled. It can be more tricky than the rest since so little power is split from the main beam path, so it might be worth amplifying the input light using the communications EDFA.

3.3 Fiber optics devices

3.3.1 Modulators

Phase modulator   An electro-optic phase modulator is an active device based on the photoelastic effect. Light going through it gains a phase $\Delta\phi = \pi\frac{V}{V_\pi}$ when a voltage V is applied. Here V_π is the voltage at which this added phase is π, and depends on the incoming light's wavelength and the properties of the crystal. In this setup it is used to add to the phase of an input optical signal the oscillations of an input AC electrical wave. If the electrical input is a sine wave $V = V_m \sin\omega_m t$ and the optical signal is $Ae^{i\omega t}$, then the output signal is

$$Ae^{i\omega t - i\frac{V_m}{V_\pi}\pi\sin(\omega_m t)} = A\sum_{n=-\infty}^{\infty} J_n(\delta)e^{i(\omega - n\omega_m)t} \tag{3.1}$$

$$\approx A\left(e^{i\omega t} + \frac{\delta}{2}e^{i(\omega+\omega_m)t} - \frac{\delta}{2}e^{i(\omega-\omega_m)t}\right) \tag{3.2}$$

with the expansion in Bessel functions of the first kind, $\delta = \pi\frac{V_m}{V_\pi}$ and where the last approximation is in first order in δ [14]. We have dropped the constant phase added by crossing the crystal $i\frac{\omega}{c}n_0 l$. In our setup, the frequency applied to the phase modulator corresponds to the difference between pump and probe frequency. It is swept around the believed Brillouin frequency of the measured crystal, with a voltage that maximizes the power in the sidebands since we will anyways filter away all the bands except the J_{-1} one.

Intensity modulator   An intensity modulator is a device that acts like a Mach-Zehnder interferometer with a free-flight arm and an arm with a phase modulator. The interference between the base signal and its phase-modulated counterpart allows one to chose how much power goes into the main band or the sideband. The total power output curve follows the following law :

$$\frac{I_o}{I_i} = \sin^2\left(\frac{\pi}{2}\frac{V}{V_\pi}\right) \approx \frac{1}{2}(1 + \Gamma_m \sin\omega_m t) \tag{3.3}$$

where V_π is the voltage at which the transmission is maximum and using using $V = \frac{V_\pi}{2} + \Gamma_m \sin \omega_m t$. While one could compute V_π using the properties of the crystal and the light, it is usually simply measured. Around $V = \frac{V_\pi}{2}$, the intensity modulation is very close to being linear in the applied voltage. Hence, in order to translate a periodic signal from applied AC voltage to amplitude modulation as close as possible, one applies a DC voltage to get to this linear regime, then adds a comparatively weaker AC voltage at the wanted frequency, which is what motivated the choice of V in the last step of equation 3.3.

An issue with most intensity modulators is V_π does not remain constant but is instead subject to drifting from temperature or charge effects. In that regard, it is common practice to connect the intensity modulator to a feedback loop that continuously adjusts the DC voltage input to stay in the quasilinear regime.

3.3.2 Fiber Bragg Gratings (FBGs) and narrowband filter

A fiber Bragg grating is a piece of fiber with a periodic jump between two different refractive indices [14]. The grating effectively creates a band-pass filter in reflection of the device. The reflection spectrum of a FBG can be seen in green on figure 3.4 a. By adding a gap in the grating of the right size, one can effectively create a transmission peak in the middle of the dip, creating a spectrum like the magenta one on figure 3.4.a and both green and magenta on figure 3.4.b. These so called π-shifted Bragg grating are useful when one wants to suppress a signal's immediate spectral surroundings for example.
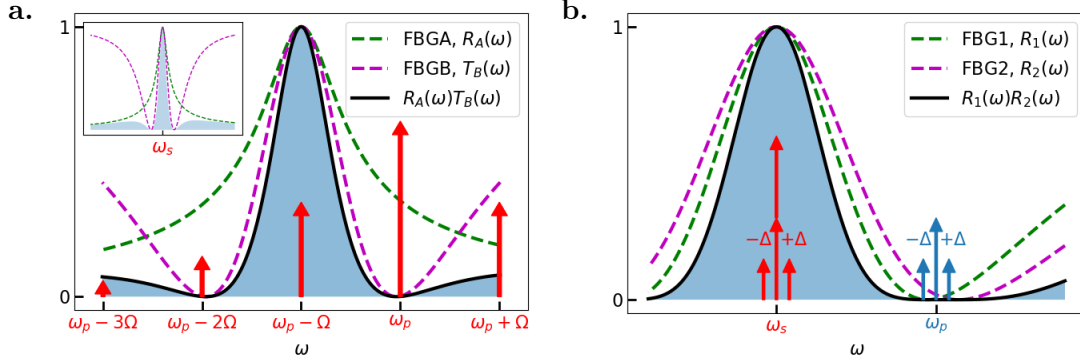

Figure 3.4: Illustration of the filtering in the (a) Probe arm using the transmission of a π-shifted FBG and the reflection of a regular FBG with an inset showing an extended spectrum of these two FBGs and in the (b) output arm using the transmission of two π-shifted FBGs. See 4.2 for actual spectra out of measurements.

Probe arm In the probe arm, we use an iXblue ultra-narrow band filter aimed around $\omega_p - \Omega_B$ to select the wanted Stokes frequency at the -1 sideband of the phase modulated

pump light. The filter's band needs to be narrower than the modulation frequency, but as broad as the extent of the modulation frequency sweep. This narrowband filter is an integrated device incorporating two FBGs and a circulator. The light that comes out is the reflection of a regular FBG and the transmission of a π-shifted one.

The π-shifted FBG suppresses the immediate surroundings of the signal with a narrowness of bandwidth hard to attain with regular FBGs, but also lets further light through. On the other hand, the regular FBG has a broader transmission center but suppresses light further away with depth close to 1, as can be seen in the inset of figure 3.4.a. The spectra are drawn using simple formulae extracted, for example in [15], using the transfer matrix method developed in [16].

Output arm   In the output arm, the light is transmitted through two π-shifted FBGs in a row to suppress 60 dB out of the backreflected pump light. These FBGs have their center on ω_s so they let the light at this frequency through while suppressing the pump light through as can be seen on figure 3.4.b. They are used on transmission and not reflection because, as will be shown in section 4.1, we have observed a much better filtering depth in this configuration. A drawback in using them on reflection is they do not suppress light further away in both directions.

These filters' bandwidth also determine an upper bound for the intensity modulator's AC input frequency, in the of 100s of kHz, much smaller than the Brillouin frequency. The two limits on the intensity modulator's applied voltage frequency are then the bandwidth of the output filters (~ 1 GHz) and the condition for signature imprinting $\frac{v_o}{\Delta} \gg L$. At $\Delta \sim 100$ kHz, we indeed have $\frac{v_0}{\Delta} = \frac{c}{n_{\text{quartz}}\Delta} \approx 2\text{m} \gg 5\text{mm}$. The FBGs are separated by an optical isolator to avoid creating an optical cavity between them.

3.3.3 EDFAs

The output Stokes signal power is directly dependent on the input pump power. Hence, we use a communication EDFA to increase this power up to (200 mW, ~ 23 dBm). After splitting, modulating and filtering, the probe power is usually very weak, so we also use an EDFA on this arm to go from -10 to 12 dBm. The initial power of the laser is sufficiently high and the losses of the fibers optic setup prior to the freespace optics sufficiently low to avoid the need for amplification of the laser light at the beginning of the setup.

3.4 Measurement scheme

The light coming out of the output arm of the free space setup features some backreflected pump light at frequencies ω_p, $\omega_p \pm \Delta$, transmitted probe light at frequency ω_s and the Brillouin signal, or amplified probe light, at frequencies ω_s, $\omega_s \pm \Delta$ on first approximation. The goal of the following section is to show how we isolate and measure this last signal.

3.4.1 Balanced detection

After the filtering discussed in section 3.3.2, the light in the output arm still has some transmitted probe light in addition to the Brillouin signal. To increase sensitivity and ensure we are only measuring the Brillouin signal, we divert some probe light before it enters the free-space setup, and have it go through a variable optical attenuator (VOA) to power-match it to the output light, which is typically much weaker. The Thorlabs PDB415C detector measures both the output light and this diverted probe light and outputs the difference of the two signals' power (RF output), but also each individual signal, which is very convenient for power matching. Once balanced, the RF output is sent to the lock-in amplifier.

3.4.2 Lock-in amplification

A lock-in amplifier is an electrical device that very effectively isolates a signal from a noisy environment by mixing it with a reference signal of the same frequency, and filtering out the fast-rotating components of the resulting signal. The first step, called demodulation, consists in multiplying the signal $V_s(t) = \frac{R}{\sqrt{2}}e^{i(\omega_s t + \theta)} + \frac{R}{\sqrt{2}}e^{-i(\omega_s t + \theta)}$ by a reference signal of close or equal frequency $\sqrt{2}e^{i\omega_r t}$ to get the resulting signal

$$Z(t) = R \left(e^{i((\omega_s - \omega_r)t + \theta)} + e^{-i((\omega_s + \omega_r)t + \theta)} \right). \tag{3.4}$$

By applying a low-pass filter of sufficient depth, we can get rid of the fast-rotating component $|\omega_s + \omega_r|$. In the case $\omega_s = \omega_r$ we simply get R as an output, i.e. the amplitude of the signal [17].

Results

4.1 Filtering depth

Using the sweep capacities of the Santec TSL-710 laser and the Santec MPM-210 power meter, we were able to obtain precise spectrum of the two filters used in the setup. The results can be seen on figure 4.1. As one can see, the filtering depth of π-shifted FBGs is better on transmission than on reflection, by a factor 2. On both these filters, the depth can reach up to -60 dB, but the bandwidth is larger than the modulation frequency on the bandpass filter picture, leading to suboptimal filtering. It could be made better by bettering the alignment of the two FBGs, or moving the light slightly to the blue, accepting a lesser transmission of probe light but removing all of the pump light.
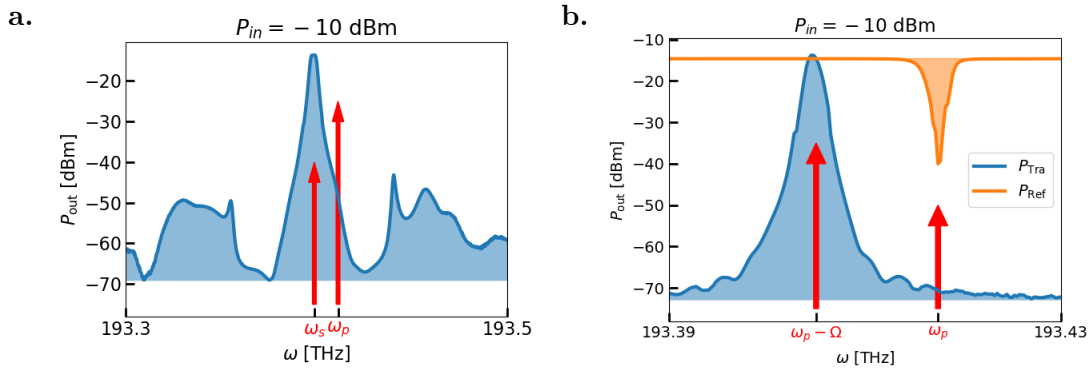

Figure 4.1: Results of the filtering depths measurements. (a) The Bandpass filter has a maximum depth of 60 dB but only 40 where we are using it, while the (b) double FBGs on output arm have a depth of 30 dB when used on reflection versus 60 dB on transmission.

4.2 Brillouin signal in optical fiber

In order to test a part of the setup, we can remove the free-space optical isolator in front of the probe coupler, thus allowing Brillouin scattering to take place in the fiber connecting to it. We know the frequency of maximum amplification is 10.85 GHz in optical fiber. We sweep the phase modulator's RF input between 10.6 and 11.1 GHz and

look at the lock-in amplified signal. The Brillouin signal can be seen as peaks on figure 4.2, representing the demodulated output from the balanced detector in the situation described above. At the time of creating this figure, the setup did not allow for access to the frequency of the generator to have x-axis, so instead only the time is shown.
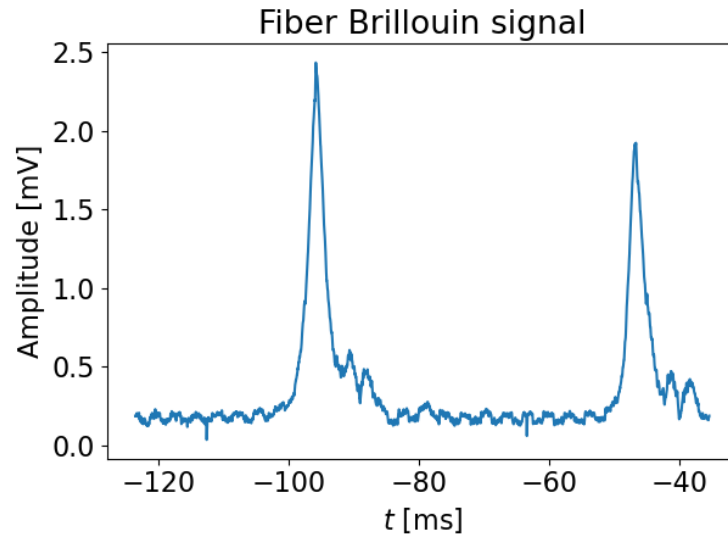

Figure 4.2: Fiber Brillouin signal in the demodulated output of the balanced detector over 2 sweeps of the probe arm phase modulator's RF input frequency.

Outlook

In this report, we have successfully set up all the components of a Brillouin spectrometer, and measured the first proof of its capabilities with a fiber Brillouin signal. We have covered the basic theory behind most of the components and how they are used and mounted in this setup. Once fully and, as much as possible, automatically functioning, this setup will make for easier experiments using Brillouin scattering in bulk crystalline media inside of dilution refrigerators by accurately giving their Brillouin frequency. Once fine tuned for efficiency, it could additionally give expected Brillouin gain of these media, as well as these two quantities' temperature dependency, from 300 to 4.2 K.

Bibliography

1. Andrews, R. W. *et al.* Bidirectional and efficient conversion between microwave and optical light. en. *Nature Phys* **10,** 321–326. ISSN: 1745-2473, 1745-2481. `http://www.nature.com/articles/nphys2911` (2021) (Apr. 2014).

2. Forsch, M. *et al.* Microwave-to-optics conversion using a mechanical oscillator in its quantum ground state. en. *Nat. Phys.* **16,** 69–74. ISSN: 1745-2473, 1745-2481. `http://www.nature.com/articles/s41567-019-0673-7` (2021) (Jan. 2020).

3. Wu, M., Zeuthen, E., Balram, K. C. & Srinivasan, K. Microwave-to-Optical Transduction Using a Mechanical Supermode for Coupling Piezoelectric and Optomechanical Resonators. en. *Phys. Rev. Applied* **13,** 014027. ISSN: 2331-7019. `https://link.aps.org/doi/10.1103/PhysRevApplied.13.014027` (2021) (Jan. 2020).

4. Mirhosseini, M., Sipahigil, A., Kalaee, M. & Painter, O. Superconducting qubit to optical photon transduction. en. *Nature* **588,** 599–603. ISSN: 0028-0836, 1476-4687. `http://www.nature.com/articles/s41586-020-3038-6` (2021) (Dec. 2020).

5. Fiore, V., Dong, C., Kuzyk, M. C. & Wang, H. Optomechanical light storage in a silica microresonator. en. *Phys. Rev. A* **87,** 023812. ISSN: 1050-2947, 1094-1622. `https://link.aps.org/doi/10.1103/PhysRevA.87.023812` (2021) (Feb. 2013).

6. Chu, Y. *et al.* Creation and control of multi-phonon Fock states in a bulk acoustic-wave resonator. en. *Nature* **563,** 666–670. ISSN: 0028-0836, 1476-4687. `http://www.nature.com/articles/s41586-018-0717-7` (2021) (Nov. 2018).

7. Aspelmeyer, M., Kippenberg, T. J. & Marquardt, F. Cavity optomechanics. en. *Rev. Mod. Phys.* **86,** 1391–1452. ISSN: 0034-6861, 1539-0756. `https://link.aps.org/doi/10.1103/RevModPhys.86.1391` (2021) (Dec. 2014).

8. O'Connell, A. D. *et al.* Quantum ground state and single-phonon control of a mechanical resonator. en. *Nature* **464,** 697–703. ISSN: 0028-0836, 1476-4687. `http://www.nature.com/articles/nature08967` (2021) (Apr. 2010).

9. Arrangoiz-Arriola, P. & Safavi-Naeini, A. H. Engineering interactions between superconducting qubits and phononic nanostructures. en. *Phys. Rev. A* **94,** 063864. ISSN: 2469-9926, 2469-9934. `https://link.aps.org/doi/10.1103/PhysRevA.94.063864` (2021) (Dec. 2016).

10. Ockeloen-Korppi, C. F. *et al.* Stabilized entanglement of massive mechanical oscillators. en. *Nature* **556,** 478–482. ISSN: 0028-0836, 1476-4687. `http://www.nature.com/articles/s41586-018-0038-x` (2021) (Apr. 2018).

11. Riedinger, R. *et al.* Remote quantum entanglement between two micromechanical oscillators. en. *Nature* **556,** 473–477. ISSN: 0028-0836, 1476-4687. `http://www.nature.com/articles/s41586-018-0036-z` (2021) (Apr. 2018).

Bibliography

12. Renninger, W. H., Kharel, P., Behunin, R. O. & Rakich, P. T. Bulk crystalline optomechanics. en. *Nature Phys* **14,** 601–607. ISSN: 1745-2473, 1745-2481. `http://www.nature.com/articles/s41567-018-0090-3` (2021) (June 2018).

13. Boyd, R. W. *Nonlinear optics* 3rd ed. ISBN: 978-0-12-369470-6 (Academic Press, Amsterdam ; Boston, 2008).

14. Yariv, A., Yeh, P. & Yariv, A. *Photonics: optical electronics in modern communications* 6th ed. OCLC: ocm58648003. ISBN: 978-0-19-517946-0 (Oxford University Press, New York, 2007).

15. Rosenthal, A., Razansky, D. & Ntziachristos, V. High-sensitivity compact ultrasonic detector based on a pi-phase-shifted fiber Bragg grating. *Opt. Lett.* **36,** 1833–1835. `http://ol.osa.org/abstract.cfm?URI=ol-36-10-1833` (2011).

16. Erdogan, T. Fiber grating spectra. *Journal of Lightwave Technology* **15,** 1277–1294 (1997).

17. Zürich-Instruments. Principles of lock-in detection and the state of the art.